Research Article

IJUSEng – 2013, Vol. 1, No. 3, 48-67
http://dx.doi.org/10.14323/ijuseng.2013.12

Advanced Flight Management System for an Unmanned Reusable Space Vehicle

Manoj Sangam [1], *Roberto Sabatini* [2] ✉, *Subramanian Ramasamy* [1] *and Alessandro Gardi* [1]

1. *Department of Aerospace Engineering, Cranfield University, United Kingdom.*
2. *School of Aerospace, Mechanical and Manufacturing Engineering, RMIT University, Australia.*

Abstract: Sangam M, Sabatini R, Ramasamy S and Gardi A. (2013). Advanced flight management system for an unmanned reusable space vehicle. *International Journal of Unmanned Systems Engineering.* ***1***(3): 48-67. The innovative architecture of an advanced Flight Management System (FMS) for Unmanned Reusable Space Vehicle (URSV) applications is presented with the associated re-entry trajectory computation algorithm. The SL-12 unmanned space vehicle, developed by Cranfield University as a part of the 2012-2013 Aerospace Vehicle Design (AVD) Group Design Project (GDP) is used as the reference platform. The overall avionics architecture of the future space transportation vehicle is described. A detailed architecture is developed for the FMS and the core functions of such an FMS are described. A dedicated computation algorithm is presented for re-entry trajectory planning, which involves determination of the path of re-entry vehicle by means of angle of attack and bank angle modulation. Simulation case studies are performed in a realistic re-entry operational scenario resulting in the generation of efficient and feasible trajectories, without violating any of the defined constraints.

Keywords:
Flight management system
Reusable launch vehicle
Trajectory optimisation
Re-entry trajectory planning

1. INTRODUCTION

Access to the airspace, conventionally prerogative to commercial aircraft, is envisaged to be gradually extended to Unmanned Aerial Vehicles (UAVs) and space transportation vehicles in the next decade. Currently, higher levels of automation of flight tasks, for both manned aircraft and autonomous robots, are primarily achieved by the deployment of Flight Management System (FMS). The primary research focus is on the design, development, test and evaluation (DDT&E) of an advanced FMS for an Unmanned Reusable Space Vehicle (URSV). Numerous methods for route planning and generation of optimal flight profiles between given waypoints or city pairs have been implemented in the FMS.[1-3] The primary objective of the FMS in the context of an URSV is trajectory planning for atmospheric re-entry.

Correspondence
RMIT University
SAMME Reception
Building 57, Level 3, Office 36
114 Queensberry Street
Carlton, VIC 3053, Australia
roberto.sabatini@rmit.edu.au
www.rmit.edu.au

The Space Shuttle's entry guidance system[4] is based on the creation of a drag acceleration profile and is proven to be highly successful. Angle of Attack (AoA) and bank angle modulation are used for keeping the shuttle along the planned profile. A limitation of shuttle entry guidance is that the reference entry profile is not generated on-board. Hence, abort scenarios have to be designed pre-mission and it is difficult to incorporate off-nominal conditions.

An entry trajectory planner that generates a feasible trajectory and associated bank angle profile, demonstrating significant improvement in performance has been proposed.[5] In [6] an algorithm for on-board generation of Three-Degree-of-Freedom (3DOF) entry trajectories satisfying all the path constraints has been proposed. This approach is based on the quasi-equilibrium glide condition and is capable of autonomously generating reference trajectories for any given scenario. The design and performance evaluation of an entry guidance algorithm to plan and track aerodynamic acceleration has been employed for space transportation vehicles.[7] A methodology for re-entry trajectory planning, which is essentially an extension of the shuttle entry guidance, has been developed.[8,9] This approach overcomes the limitations of the shuttle re-entry guidance, at the same time retaining the best features of the shuttle re-entry. Hence, this method is used as a baseline for defining re-entry trajectory planning algorithm for the space vehicle considered in this paper.

2. REUSABLE SPACE VEHICLE

2.1. Introduction to the Platform: SL-12

Novel and improvised ways of space transportation are being researched upon to explore suitable alternatives to Space Shuttle. Cranfield University's 2012-2013 Aerospace Vehicle Design (AVD) project brainchild "SL-12" is a winged orbiter that was developed as a potential solution to future space transportation, and is reconfigurable as well as reusable. Further, this URSV has a short turn-around time and it is suitable for a variety of missions. The SL-12 spacecraft is envisaged to be operational by 2020. The SL-12 is designed in accordance with the guidelines defined for both space vehicles as well as commercial aircraft.[10–12] A Computer-Aided Design (CAD) model of the space transportation vehicle SL-12 is illustrated in Fig. 1.

Fig. 1: CAD model of SL-12 winged orbiter

According to the project specification[13], the SL-12 URSV would be launched from an expendable launcher system such as Delta-IV or Atlas-V. The SL-12 would be used to perform a wide range of operations such as:

- Carry and launch satellites into Low Earth Orbit (LEO).
- Transfer crew to and from the International Space Station (ISS).
- Deliver a payload to / retrieve a payload from the ISS.
- Remain in orbit for 2 years and act as a 'reusable satellite'.

The various avionics systems on-board the SL-12 are depicted in Fig. 2.

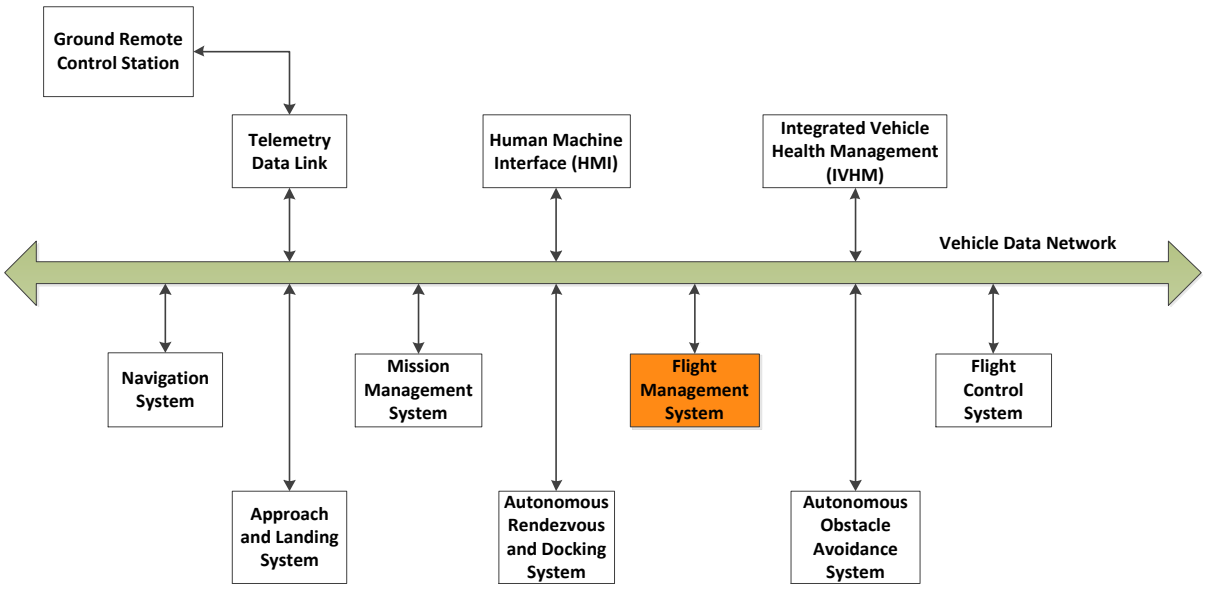

Fig. 2: SL-12 global avionics architecture

The SL-12 avionics is composed of the following sub-systems:

- **Flight Management System:** The FMS primarily performs trajectory determination for the atmospheric flight. Specifically, the FMS retains the URSV within the entry-corridor during atmospheric re-entry and performs energy management to ensure a safe landing.

- **Mission Management System (MMS):** The MMS carries out strategic level mission planning and execution. These tasks involve orbit determination, calculation of difference in velocity (ΔV) for orbit transfers and delivery / retrieval of payload. The MMS also issues 'mission abort' command in cases of emergency.

- **Navigation System:** The objective is to design an integrated navigation system by data fusion from inertial sensors, Global Navigation Satellite System (GNSS), radar, infrared cameras, air data sensors and other candidate sensors. The navigation system provides position, attitude and velocity of the URSV in three dimensions.

- **Flight Control System (FCS):** The FCS comprises reaction control system for attitude control during space flight and aerodynamic control system for vehicle control during atmospheric flight. Robust control laws are developed to improve the stability and controllability of the URSV in all flight phases.

- **Human Machine Interface (HMI):** The HMI component controls all the on-board display systems, as well as the interfaces for crew control.

- **Approach and Landing System:** This component addresses the design of an autonomous approach and landing system, whose operation is based on navigation facilities such as the Microwave Landing System (MLS). It is the responsibility of this system to steer the vehicle towards the runway from the approach and landing phase.

- **Integrated Vehicle Health Management System (IVHM):** The IVHM performs on-board fault diagnostics and system reconfiguration in case of failures.

- **Telemetry Data Link:** The telemetry data link ensures the communication of the URSV mission data to the ground remote control station and to the space station.

- **Ground Remote Control Station (GRCS):** The GRCS component continuously tracks the URSV and provides mission specific commands via the established telemetry data link.

- **Autonomous Obstacle Avoidance System:** This component detects the space debris in the orbit, other aircraft / terrain conflicts in the atmosphere and alerts the FMS about a probable collision. Furthermore, a collision avoidance manoeuvre is performed based on the guidance commands from the FMS, which are based on the inputs from the autonomous obstacle avoidance system.

- **Autonomous Rendezvous and Docking System:** This component involves the calculation of the relative position of the URSV with respect to a given space station, guiding the spacecraft towards the space station and facilitating docking with the respective space station.

3. ARCHITECTURE OF THE FMS OF AN URSV

The space vehicle SL-12 is the reference platform to develop the architecture of the FMS and to demonstrate the entry trajectory planning algorithm. In case of a spacecraft, the task of trajectory planning and guiding the vehicle along the desired trajectory is performed by the Guidance, Navigation and Control (GNC) system[14-17]. A launcher system inserts the URSV into the desired orbit. During the space flight, the FMS just oversees the orbital manoeuvres. The real operation of the FMS begins after de-orbiting. During the atmospheric flight, the FMS oversees the trajectory generation and steering of the vehicle from the start of re-entry point till approach and landing interface. Hence, the focus of this paper is trajectory planning for atmospheric re-entry. Fig. 3 illustrates the detailed functional architecture of the FMS of an URSV.

The core functions of the FMS of an URSV are described below:

- **Navigation Database:** the navigation database stores the waypoints information, location of the navigation aids, runway information and mission specific data. Waypoint information consists of coordinates of the Terminal Area Energy Management (TAEM) interface, heading alignment cylinder, approach and landing interface and the runway. Mission specific data refers to altitude and inclination of target orbits and point of de-orbit.

- **Performance Database:** this module is of paramount importance so that the vehicle stays within the re-entry flight corridor during re-entry and reaches the TAEM interface within a specified threshold. This requirement dictates that all the path constraints and URSV performance limits are stored in a database in a systematic way, to facilitate accurate trajectory predictions and robust guidance. Hence, the performance database consists of the following attributes:

    - *Aerodynamic characteristics:* tabular data for lift and drag coefficients as a function of AoA and Mach number.
    - *Path constraints:* table of path constraints; namely, maximum heat flux, maximum g-loads, and maximum dynamic pressure.
    - *Orbiter envelope*: table including maximum AoA and bank angle that can be applied, and their rate of change
    - *Vehicle data:* table including vehicle specific data such as mass of the vehicle, maximum payload weight, wing reference area, and radius of the nose.
    - *Target conditions:* table specifying the TAEM interface conditions; namely, desired altitude, velocity, and heading at the TAEM interface.

- **Re-entry Trajectory Planning:** the core module of the FMS is the re-entry trajectory planning. The hypersonic re-entry phase begins at an altitude of 120 km where the speed of the URSV would be around Mach 25. The primary objective of this phase is to dissipate excess energy, reduce the speed of the URSV and convey it to the TAEM interface with the specified conditions.

    - The first step in trajectory generation is fetching the mission profile data from the navigation database consisting of orbital inclination, time of de-orbit, projected entry altitude, and entry velocity.
    - The current position of the URSV in three dimensions is obtained from the navigation system.
    - The path constraints and performance limits are acquired from the performance database.
    - Based on the entry conditions and imposed constraints, a reference trajectory is generated by the FMS comprising of altitude-velocity profile, drag acceleration profile, and desired AoA and bank angle profiles.

- **Terminal Area Energy Management:** the TAEM is the penultimate phase in the atmospheric flight, which steers the vehicle from the end of re-entry phase (initiated when the altitude was about 25 km and the speed was around Mach 2.5) to the approach and landing interface (with an altitude of 3 km and speed of Mach 0.5). The purpose of this phase is to optimally manage the energy of the URSV and ensure landing on the specified runway.

- **Performance Monitoring:** this module of the FMS continuously monitors the energy of the URSV and if there is excess energy, it initiates energy dissipating banking turns. On the other hand, if the energy is lower than required, it increases the rate of descent.

- **Fault Management:** this function performs the power-up test on system initialization and additional functions like integrity management of the GNSS signal on insertion into the orbit. Additionally, it keeps track of errors which have occurred in the FMS and updates a maintenance log. On the occurrence of a fault, system reconfiguration is initiated. The fault management function also broadcasts the overall system health status on the vehicle data network.

- **Mode Selection and Display:** this module essentially provides an interface for the crew to enter the flight data and displays all the relevant flight information by interacting with the HMI system. The implemented operational modes are *orbit insertion*, *on-orbit missions*, *de-orbit*, *re-entry*, *TAEM* and *landing*. These modes can be either manually changed by the crew or automated selection could be performed.

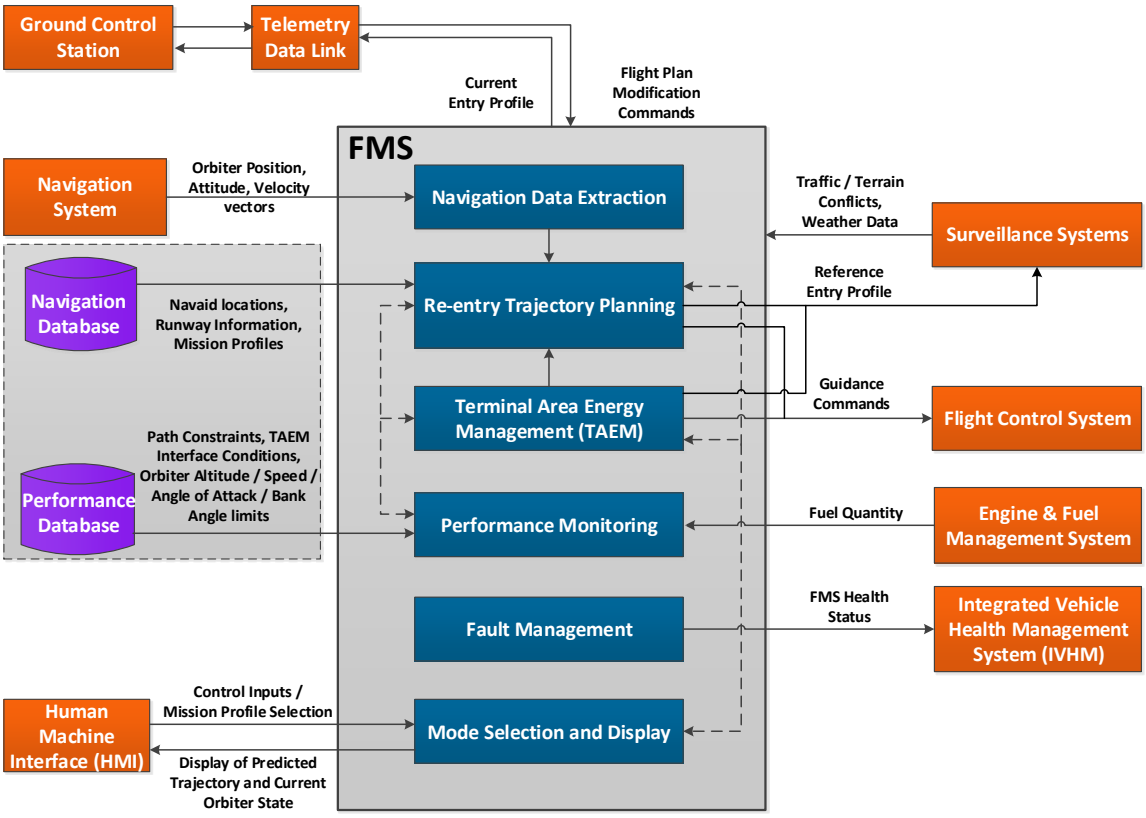

Fig. 3: Functional architecture of FMS of an URSV

4. RE-ENTRY TRAJECTORY DESIGN

4.1 Problem Definition

Given the initial re-entry conditions and target TAEM conditions, the objective is to find the states and the corresponding controls such that all the path constraints are satisfied and the URSV reaches the TAEM interface within the specified limits. Bank angle and AoA are the control variables which characterise the entry trajectory. Methods of trajectory planning for TAEM phase have been described in [14,15]. Trajectory planning for TAEM phase of SL-12 is beyond the scope of this paper.

4.2. Re-Entry Trajectory Planning Algorithm

The trajectory planning algorithm is depicted in Fig. 4.

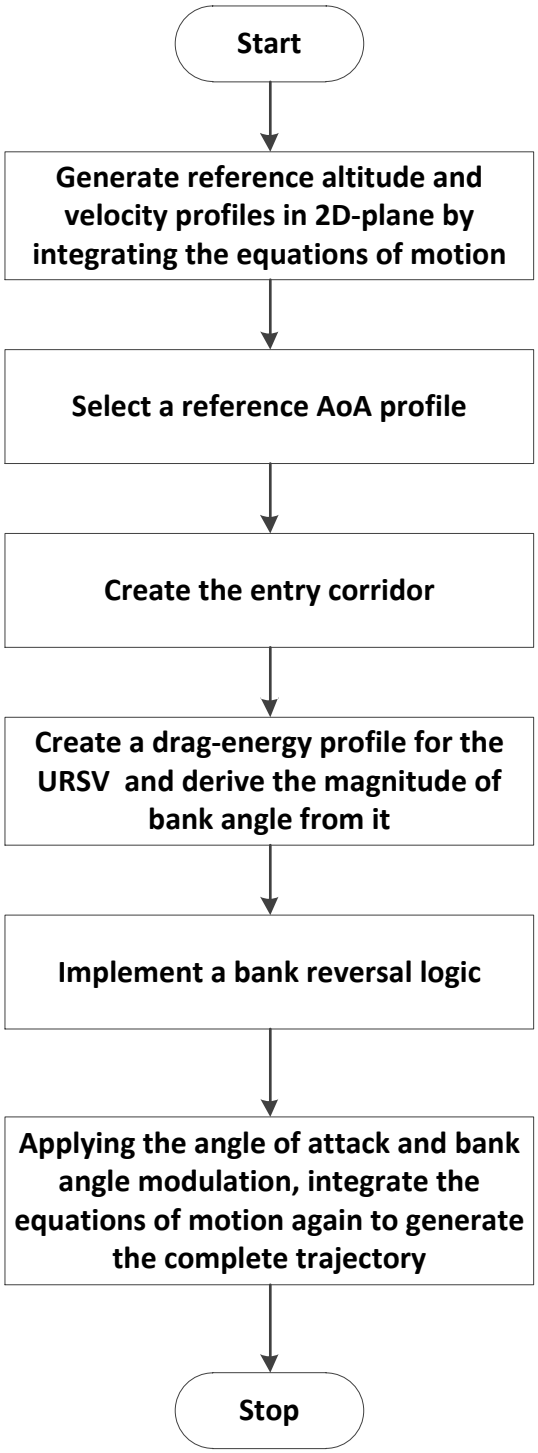

Fig. 4: Trajectory planning algorithm for re-entry

Reference altitude and velocity profiles are generated in the Two-Dimensional (2D) plane by integrating the Equations of Motion (EoM). A reference AoA profile is selected. An energy corridor is constructed with specific upper and lower boundaries. A drag-energy profile is created and it is used for deriving the magnitude of the bank angle. The direction of bank angle is reversed whenever the heading of the vehicle with respect to TAEM interface exceeds a predefined threshold. With the sign of bank angle so obtained, the trajectory is propagated till TAEM interface and the cross-range attained at TAEM interface is

determined. The objective of bank reversal logic is to minimize the cross-range error. By applying AoA and bank angle modulation and integrating the EoM, the complete trajectory is generated.

4.3 Equations of Motion for the URSV

A 3DOF point mass model is used as the Aircraft Dynamics Model (ADM). The 3DOF EoM describing the aircraft states and governing the translational movements along the longitudinal, lateral and vertical axes are:

$$\dot{r} = V \sin\gamma \tag{1}$$

$$\dot{\theta} = \frac{V \cos\gamma \sin\psi}{r \cos\varphi} \tag{2}$$

$$\dot{\varphi} = \frac{V \cos\gamma \cos\psi}{r} \tag{3}$$

$$\dot{V} = -D - (\sin\gamma \ / \ r^2) \tag{4}$$

$$\dot{\gamma} = \left(\frac{1}{V}\right)\left[L\cos\sigma + \left(V^2 - \frac{1}{r}\right)\left(\frac{\cos\gamma}{r}\right)\right] \tag{5}$$

$$\dot{\psi} = \left(\frac{1}{V}\right)\left[\left(\frac{L\sin\sigma}{\cos\gamma}\right) + \left(\frac{V^2}{r}\right)(\cos\gamma \ \sin\psi \tan\varphi)\right] \tag{6}$$

where, r is the radial distance from the centre of the Earth to the URSV in meters, θ is the geodetic longitude in radians, φ is the geodetic latitude in radians, V is the Earth relative velocity in m/s, D and L are the aerodynamic drag and lift accelerations in m/s^2, γ is the flight path angle in radians, σ is the bank angle in radians and ψ is the azimuth angle in radians. The EoM incorporate two control variables $\mathbf{u} = [\sigma, \alpha]$ where α is the angle of attack and is implicitly comprised as part of the aerodynamic accelerations. The six state variables are described as $\mathbf{x} = [r, \theta, \varphi, V, \gamma, \psi]$, the derivatives of which are presented in the EoM. For conciseness, the effects of wind and other atmospheric disturbances are neglected in this paper. However, as described in [16–18], these effects can be incorporated in the analysis at a successive stage without detracting from the general applicability of the results.

The lift and drag accelerations are given by:

$$L = \left(\frac{1}{2}\right)\frac{\rho V^2 S_{ref} C_L}{m} \tag{7}$$

$$D = \left(\frac{1}{2}\right)\frac{\rho V^2 S_{ref} C_D}{m} \tag{8}$$

where, ρ is the atmospheric density in kg/m^3, S_{ref} is the reference surface area of the URSV in m^2, C_L is the lift coefficient, C_D is the drag coefficient, m is the mass of the vehicle in kg and g_0 is the gravitational acceleration at the Earth's surface, that is $g_0 = 9.81\ m/s^2$. With the assumptions of no side-slip, non-rotating Earth and motion in vertical plane only, the EoM are simplified as follows[19]:

$$\dot{r} = \dot{h} = V_i \sin\gamma \tag{9}$$

$$\dot{V}_i = -\left(\frac{D}{m}\right) - (g \sin\gamma) \tag{10}$$

$$\dot{\gamma} = \left(\frac{1}{V_i}\right)\left[\frac{L}{m}\cos\sigma - \left(g - \frac{V_i^2}{r}\right)\cos\gamma\right] \tag{11}$$

where:

$$g = g_0\left(\frac{R}{R+h}\right)^2 \tag{12}$$

In the above equations, r = R + h, where R is the Earth's radius in meters, h is the height above earth's surface in meters, V_i is the inertial velocity in m/s, V is the Earth relative velocity in m/s, g is the gravitational acceleration at a defined altitude in m/s^2.

4.4. Path Constraints and Construction of Entry Corridor

The path constraints pertaining to heat flux, dynamic pressure and g-load form the upper boundary of the entry corridor. In general, we have:

$$\dot{Q} \leq \dot{Q}_{max} \tag{13}$$

$$|L\cos\alpha + D\sin\alpha| \leq n_{max} \tag{14}$$

where, $\dot{Q}_{max}$ is the max heat flux in W/m^2, n_{max} is the max g-load in m/s^2. The equations for path constraints can be expressed in terms of drag acceleration as follows[9]:

$$D < \frac{\dot{Q}_{max}^2 C_D S_{ref}}{2m\, C^2 V^{2(c_2-1)}} \tag{15}$$

$$D < \frac{n_{max}\, g}{\frac{C_L}{C_D}\cos\alpha + \sin\alpha} \tag{16}$$

$$D < \frac{q_{max} C_D S_{ref}}{m} \tag{17}$$

where, q_{max} is the max dynamic pressure in N/m^2. The constant C is given by[9]:

$$C = \frac{c_1}{\sqrt{R_n\, \rho_0}}\,\frac{1}{{V_c}^{c_2}} \tag{18}$$

where, c_1, c_2 are atmospheric constants. $c_1 = (1.06584)\ 10^8\ \mathrm{W/m^{3/2}}$ and $c_2 = 3$. $V_c = \sqrt{g.r}$ is the circular velocity in m/s, ρ_0 is the Atmospheric density at sea level in $\mathrm{kg/m^3}$ and R_n is the vehicle nose radius in m.

The lower boundary of the corridor is formed by the drag corresponding to minimum lift and is given by [9]:

$$D > \left(g - \frac{V^2}{r}\right) \frac{C_D}{C_L} \tag{19}$$

4.5. Generation of Drag-Energy Profile

The next step in trajectory planning algorithm is to generate a drag acceleration profile which lies within the entry corridor and takes into account a specified trajectory length. A 3-segment linear spline geometry is implemented for modelling the drag acceleration profile.[8] Such a spline is illustrated in Fig. 5.

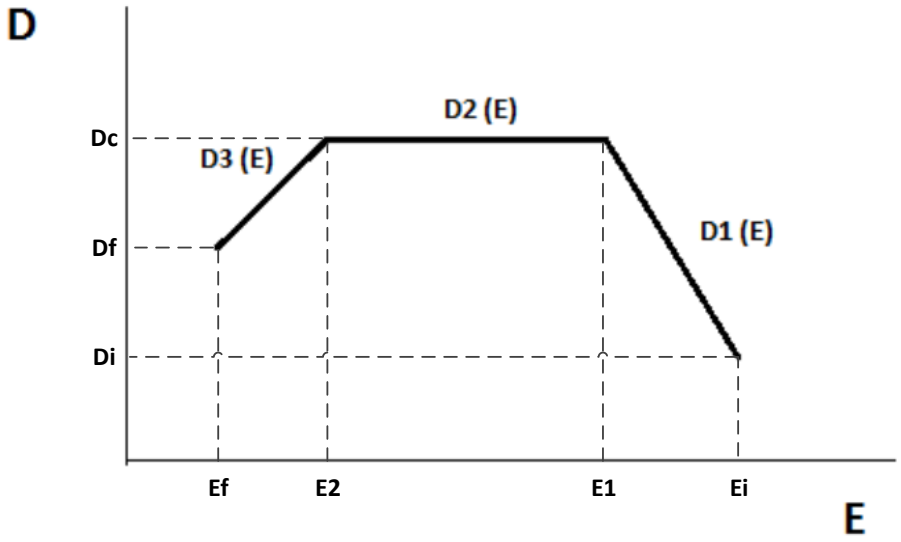

Fig. 5: Drag-energy profile modelled as 3-segment linear spline. Adapted from [9]

In the drag-energy profile, D1(E), D2(E) and D3(E) are the three drag segments. D_i and D_f are the initial and final values of drag acceleration, respectively. E_i is the initial energy at re-entry and E_f is the final energy at TAEM interface. D_c is the constant drag of the intermediate segment. E_1 and E_2 are the energies corresponding to the boundary values of the constant drag. By having prior knowledge on the altitude and velocity values at the start of re-entry and TAEM interface, all the required parameters can be determined except D_c. D_c is obtained by adopting the following method[9]:

The trajectory length which fits into this D-E profile is calculated as:

$$S = \int_0^t V\,dt = -\int_{E_i}^{E_f} \frac{1}{D(E)}\,dE \tag{20}$$

From [9], integrating the above equation for each drag segment, we obtain:

$$S = \frac{E_1 - E_i}{D_i - D_c}\ln\frac{D_c}{D_i} + \frac{E_1 - E_2}{D_c} + \frac{E_f - E_2}{D_c - D_f}\ln\frac{D_f}{D_c} \tag{21}$$

By assuming an initial estimate of trajectory length S, the only unknown variable in the above equation is D_c, which is obtained by employing the secant method. The trajectory length is the great circle arc between the entry point and the TAEM interface.

4.6. Angle of Attack Modulation

Most of the re-entry algorithms assume a nominal angle of attack profile. Though there is no specific method for determination of a reference AoA profile, a general guideline is that the AoA should be set close to the maximum value of AoA, α_{max}, during the initial part of re-entry and it should be switched to $\alpha_{(L/D)_{max}}$ at a representative altitude before TAEM interface. From the simulation tests, it was found that this representative altitude is around 45 km for the SL-12 URSV, to obtain a smooth altitude-velocity profile.

4.7. Bank Angle Modulation

The magnitude of the bank angle can be derived from the constructed drag acceleration profile. The first derivative of drag acceleration with respect to energy is given by[8,9]:

$$D' = D\left(\frac{2}{V^2} + \frac{C_D{}'}{C_D}\right) + \sin\gamma\left(-\frac{1}{\rho}\frac{\partial\rho}{\partial r} + \frac{2g}{V^2}\right) \tag{22}$$

By differentiating the above equation again with respect to energy, we get the second derivative of drag acceleration, which can be expressed in the form[9]:

$$D'' = a + b\left(\frac{L}{D}\right)\cos\sigma \tag{23}$$

where:

$$a = D\left(\frac{C_D''}{C_D} - \frac{C_D'^2}{C_D^2}\right) + D'\left(\frac{C_D'}{C_D} + \frac{2}{V^2}\right) - \frac{4D}{V^4} + \frac{1}{DV^2}\left(-\frac{1}{\rho}\frac{\partial\rho}{\partial r} + \frac{2g}{V^2}\right)\left(g - \frac{V^2}{r}\right) \tag{24}$$

$$b = -\frac{1}{V^2}\left(-\frac{1}{\rho}\frac{\partial\rho}{\partial r} + \frac{2g}{V^2}\right) \tag{25}$$

The bank angle modulation would be complete only when bank reversal logic is implemented. The approach taken for implementing bank reversal is as follows. The heading of the vehicle relative to the desired heading at TAEM interface is continuously monitored and whenever the heading of the URSV exceeds a predefined threshold, the direction of

bank angle is reversed. The space shuttle guidance system uses this strategy. The trajectory planning algorithm is iteratively solved until the smoothest possible trajectory (altitude and velocity profiles) is obtained.

5. SIMULATION AND RESULTS

The SL-12 vehicle data used for simulation is presented in Table 1. The missions and constraints data are presented in Tables 2 and 3, respectively. The SL-12 URSV vehicle is used as a platform to simulate the entry trajectory. The 1976 U.S. Standard Atmosphere Model is used to interpolate the atmospheric data such as density of air, temperature, acceleration due to gravity and speed of sound with respect to variation in altitude.

Table 1: SL-12 vehicle data

Parameter	Value
Vehicle mass with maximum internal payload	16,177 kg
Re-entry mass: Vehicle mass with maximum internal payload minus Orbital Manoeuvring System (OMS) fuel	14,186 kg
Reference surface	52.71 m^2
Nose radius	1 m

Table 2: SL-12 mission data

Parameter	Value
Entry altitude	120 km
Entry velocity	7764 m/s
TAEM altitude	24.38 km
TAEM velocity	743 m/s

Table 3: SL-12 constraints data

Parameter	Value
Maximum heat flux	964 kW/m^2
Maximum g-load	2.5 g
Maximum AoA	45°

5.1. Simulation Results

As a first step, a reference longitudinal profile (i.e., altitude / velocity profile) is generated by integrating the EoM in 2D space. Fig. 6 illustrates the simulated altitude / velocity profile. For this case, AoA was assumed to be constant at $45°$ and bank angle was set to zero.

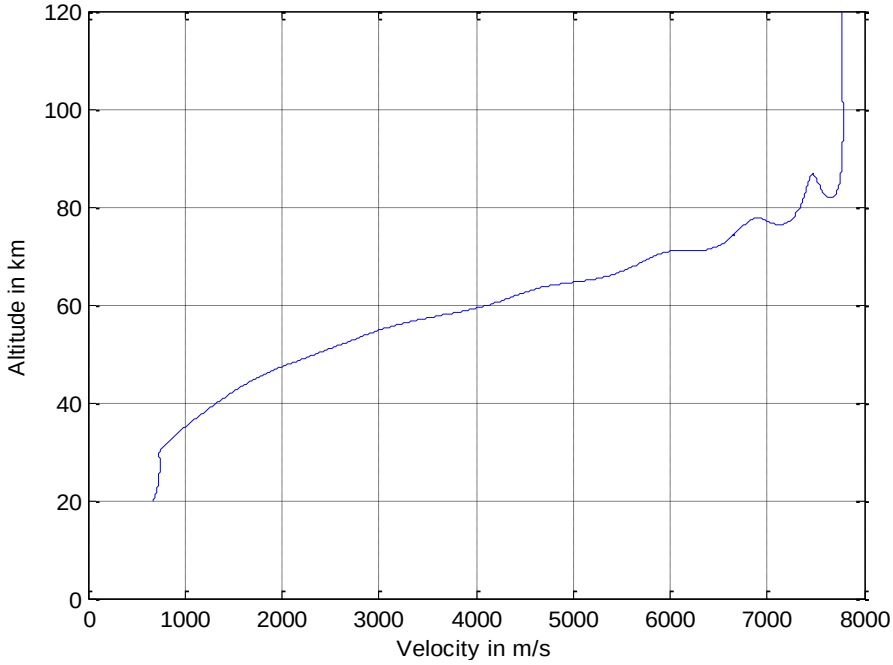

Fig. 6: Reference altitude-velocity profile

After the reference altitude-velocity profile is constructed, an entry corridor is formed in the drag-energy space and the drag acceleration profile is constructed for the vehicle under consideration, as illustrated in Fig. 7. The upper and lower boundaries of the entry corridor are shown in the Fig. 7. The upper boundary is formed by the drag accelerations corresponding to maximum heat flux and maximum g-load. The lower boundary is formed by the drag acceleration corresponding to minimum lift. The desired drag acceleration profile is constructed as a 3-segment linear spline. In the graph, x-axis indicates normalized energy, which is obtained by dividing the energy at any given instant by the nominal re-entry energy.

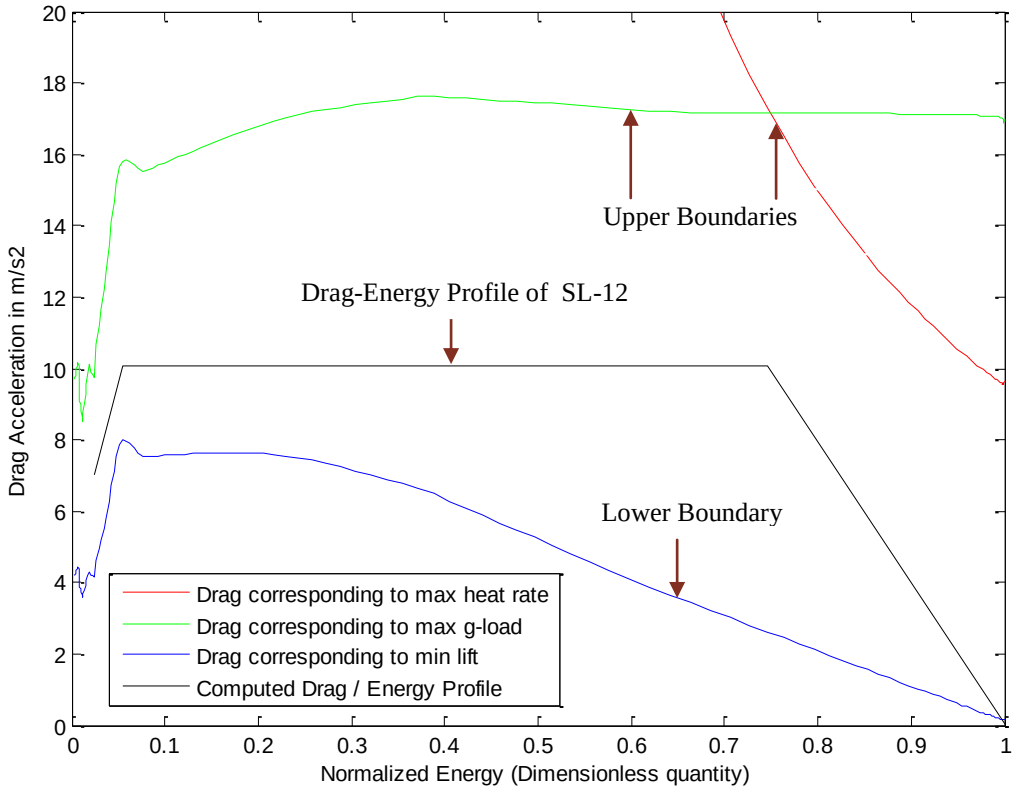

Fig. 7: Drag-energy profile for SL-12

The reference AoA and bank angle profiles are obtained after the drag-energy profile is created. The generated AoA profile is shown in Fig. 8. Angle of attack is set to a maximum of $45°$ during the initial part of re-entry to minimize heating and modulated near the TAEM interface to obtain the maximum lift-to-drag ratio.

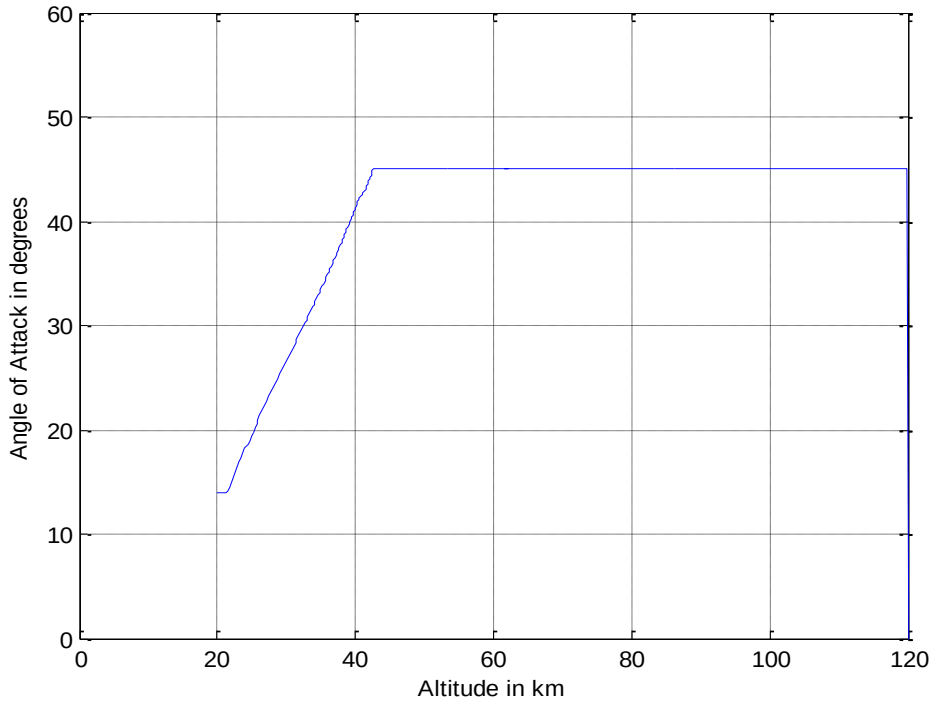

Fig. 8: Reference AoA profile

The generated bank angle profile is shown in Fig. 9. The bank angle modulation is obtained from the Drag-Energy curve.

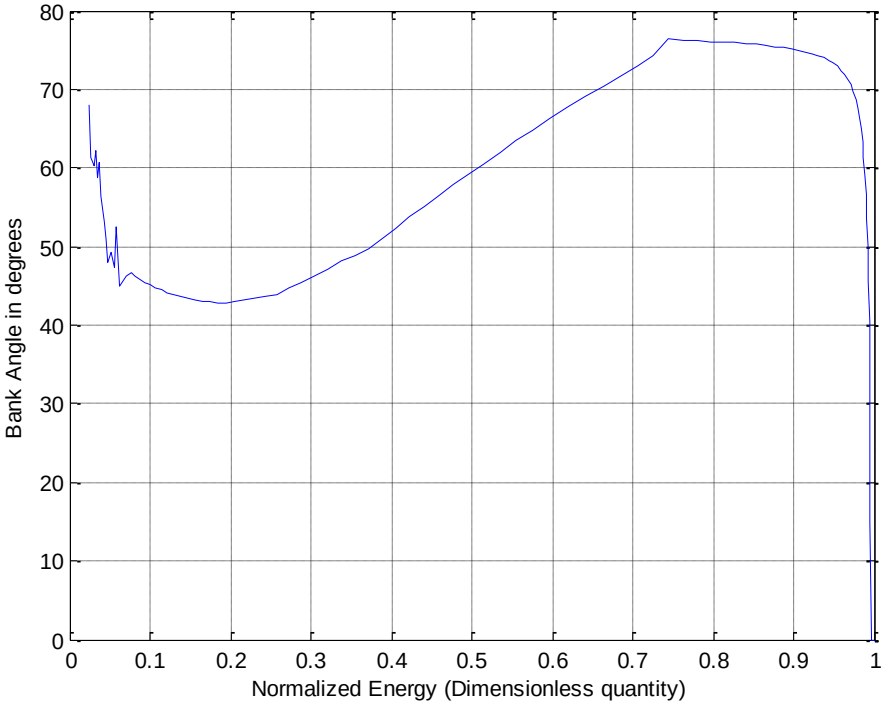

Fig. 9: Bank angle as a function of energy

Applying the angle of attack and bank angle commands as obtained above, the EoM are integrated again to generate the complete re-entry trajectory. The simulation results for the re-entry trajectory in terms of altitude and velocity profiles are shown in Figs. 10 and 11, respectively.

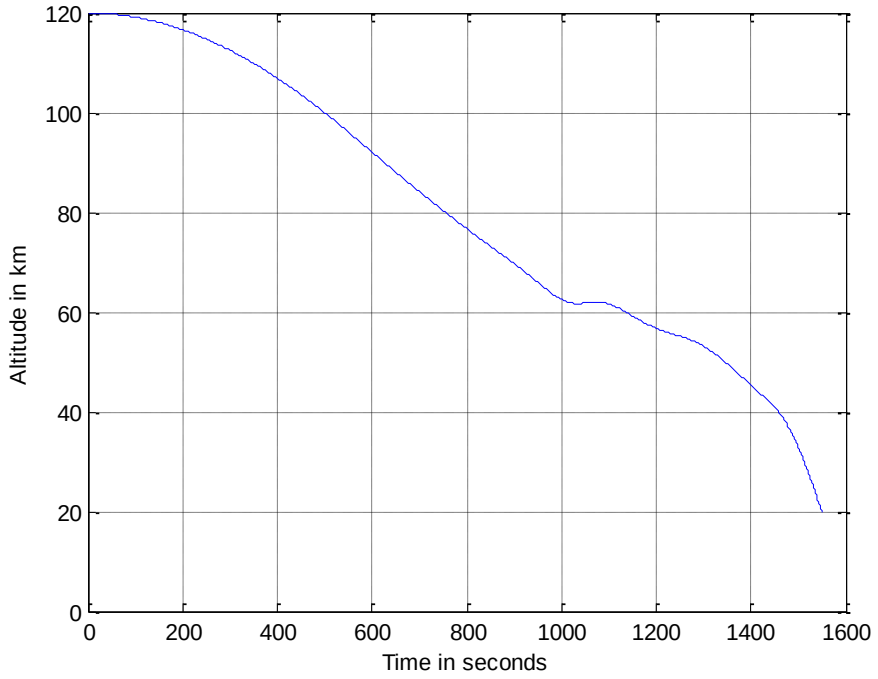

Fig. 10: Altitude profile

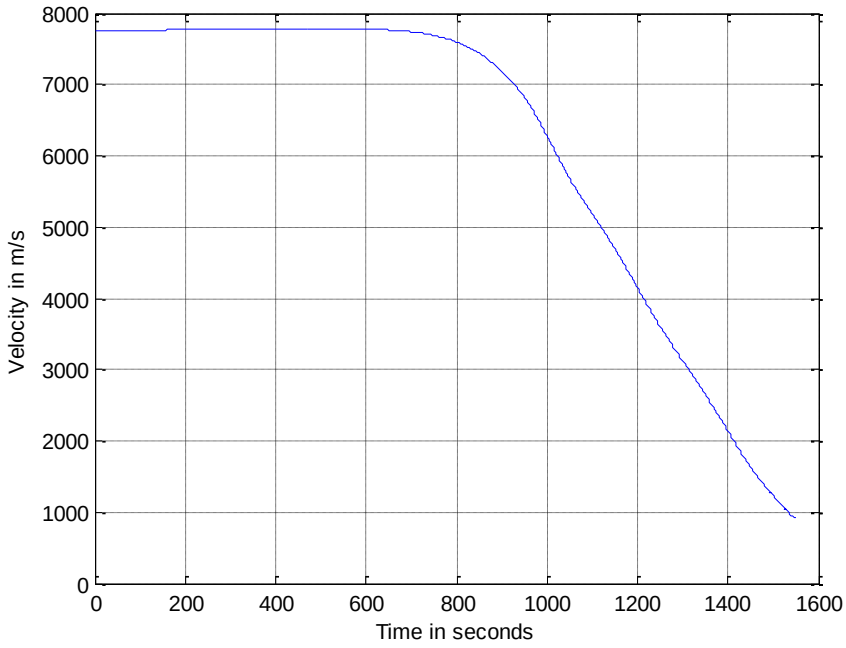

Fig. 11: Velocity profile

The altitude-velocity profile from the start of re-entry point till TAEM interface is shown in Fig. 12.

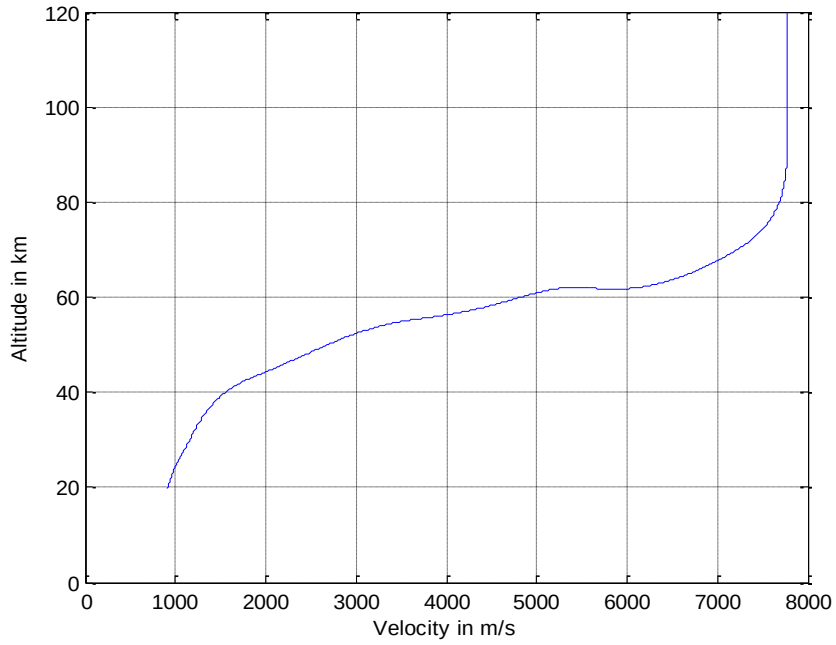

Fig. 12: Altitude-velocity profile

By comparing the plots obtained in Fig. 6 and Fig. 12, it is observed that the AoA and bank angle modulation yield a smoother trajectory and play a vital role in achieving the desired range. Fig. 11 indicates that the velocity remains constant during the first half of the re-entry phase and then decreases rapidly. The total range covered in the re-entry phase is 9378 km. The re-entry can be divided into two phases: initial descent and pseudo-equilibrium glide. Initial descent takes place from an altitude of 120 km to 80 km, where the atmospheric

density is too low. During this phase, the URSV experiences a controlled fall. Pseudo-equilibrium glide is a major portion of re-entry where lift and drag forces are sufficiently large to facilitate a lifting entry. During the pseudo-equilibrium glide, the flight path angle is very small and all of the path constraints have to be taken into account. Since there is limited authority to change the AoA over a major portion of the hypersonic re-entry, modulation of bank angle is considered as the key control parameter. In the absence of banking, when atmospheric density becomes significant, a series of sinusoidal ascents and descents occur. When banking is performed, the bank angle rotates the lift vector out of the vertical plane, thus dissipating energy sideways. Hence, banking manoeuvres provide an efficient way to dissipate excess energy, at the same time making it possible to achieve the desired range.

6. CONCLUSIONS

The design aspects of FMS of a URSV are presented in this paper. The SL-12 space vehicle, designed as part of the research activities at Cranfield University, was used as the reference platform to demonstrate concepts. A detailed architecture was developed for the FMS, with a focus on trajectory planning for atmospheric re-entry. Efforts were made to adapt the principles of FMS of a conventional aircraft to that of an URSV. Hypersonic re-entry and TAEM were identified as the two major phases of the atmospheric re-entry. The trajectory planning for these phases constitutes the core of the FMS. A novel on-board trajectory planning algorithm was developed for the hypersonic re-entry phase, which is based on the drag-energy profile. The trajectory planning algorithm presented ensures that the planned path does not violate any constraints. AoA and bank angle modulation were used to shape the re-entry trajectory. Simulation case studies were performed for the re-entry phase and the results demonstrated the capability of the developed FMS to generate efficient trajectory profiles and, at the same time, satisfying the given constraints. Future work is envisaged to address off-nominal initial and boundary conditions and abort conditions in the re-entry trajectory to improve the robustness of the design.

7. REFERENCES

1. **Liden S**. (1994). The evolution of flight management systems. *AIAA/IEEE 13th Digital Avionics Systems Conference*. 30th October – 3rd November. Phoenix. Arizona. crossref

2. **Sorensen J**. (1984). The flight planning – Flight management connection. *Proceedings of the American Control Conference*. 6th – 8th June. San Diego. California. crossref

3. **Herndon A**, **Cramer M**, **Sprong K** and **Mayer R**. (2007). Analysis of advanced flight management systems. *26th Digital Avionics Systems Conference*. 21st – 25th October. Virginia. USA. crossref

4. **Harpold J** and **Graves C**. (1979). Shuttle entry guidance. *Journal of the Astronautical Sciences.* ***37***(3): 239-268. crossref

5. **Leavitt J** and **Mease K**. (2007). Feasible trajectory generation for atmospheric entry guidance. *Journal of Guidance, Control and Dynamics*. ***30***(2): 473-481. crossref

6. **Shen Z** and **Lu P**. (2003). Onboard generation of three-dimensional constrained entry trajectories. *Journal of Guidance, Control and Dynamics.* ***26***(1): 111-121. crossref

7. **Saraf A**, **Leavitt J**, **Chen D** and **Mease K**. (2004). Design and evaluation of an acceleration guidance algorithm for entry. *Journal of Spacecraft and Rockets*. ***41***(6): 986-996. crossref

8. **Mease K**, **Chen D**, **Teufel P** and **Schonenberger H**. (2002). Reduced-order entry trajectory planning for acceleration guidance. *Journal of Guidance, Control and Dynamics*. ***25****(*2): 257-266. crossref

9. **van Doorn S**. (2010). *A mission planning tool design for re-entry*. MSc Thesis. Delft University of Technology. Netherlands. crossref

10. **NASA**. (2007). *NASA systems engineering handbook*. NASA/SP-2007-6105, Rev1. NASA Headquarters. Washington DC. USA. crossref

11. **SAE**. (2010). *Guidelines for Development of Civil Aircraft and Systems*. Aerospace Recommended Practice. ARP 4754. Rev A. Pennsylvania. USA. crossref

12. **Hanaway J** and **Moorehead R**. (1989). *Space Shuttle avionics system*. NASA-SP-504. Scientific and Technical information Division. Washington DC. USA. crossref

13. **Smith H**. (2012). SL-12 *Advanced space transportation reusable orbiter conceptual design*. Project specification. Cranfield University. Cranfield. UK. crossref

14. **Hanson J**, **Jones R** and **Krupp D**. (2002). Advanced guidance and control methods for reusable launch vehicles: Test results. *AIAA Guidance, Navigation, and Control Conference and Exhibit*. Monterey. California. USA. crossref

15. **AviDyne K**. (1968). *Guidance and navigation for entry vehicles*. NASA Space Vehicle Design Criteria. NASA SP-8015. Office of Advanced Research and Technology. Washington DC. USA. crossref

16. **Mooij E** and **Hänninen P**. (2009). Distributed global trajectory optimization of a moderate lift-to-drag re-entry vehicle. *AIAA Guidance, Navigation and Control Conference*. 10th – 13th August. Chicago. Illinois. crossref

17. **Harpold J** and **Hill O**. (1980). *MCC Level C formulation requirements for entry guidance and entry autopilot*. NASA-TM-81093. Johnson Space Centre. Texas. USA. crossref

18. **Horneman K** and **Kluever C**. (2004). Terminal area energy management trajectory planning for an unpowered reusable launch vehicle. *AIAA Atmospheric Flight Mechanics Conference and Exhibit*. Providence. Rhode Island. USA. crossref

19. **de Ridder S**. (2009). *Study on optimal trajectories and energy management capabilities of a winged re-entry vehicle during the terminal area*. MSc Thesis. Delft University of Technology. Netherlands. crossref

20. **Griffin M** and **French J**. (2004). Space vehicle design. (2nd ed.). *American Institute of Aeronautics and Astronautics*. Reston. Virginia. crossref

8. NOTATION

AVD	Aerospace vehicle design
ADM	Aircraft dynamics model
AoA	Angle of attack
CAD	Computer-aided design
DDT&E	Design, development, test and evaluation
EoM	Equations of motion
FCS	Flight control system
FMS	Flight management system
GNSS	Global navigation satellite system
GRCS	Ground remote control station
GDP	Group design project
GNC	Guidance, navigation and control

HMI	Human machine interface
IVHM	Integrated vehicle health management system
ISS	International Space Station
LEO	Low earth orbit
MLS	Microwave landing system
MMS	Mission management system
OMS	Orbital manoeuvring system
TAEM	Terminal area energy management
UAV	Unmanned aerial vehicles
URSV	Unmanned reusable space vehicle
2D	Two-dimensional
3DOF	Three-degree-of-freedom

C_D	Drag coefficient
C_L	Lift coefficient
c_1, c_2	Atmospheric constants
D	Aerodynamic drag acceleration
D_c	Drag acceleration of the intermediate segment
D_f	Final value of drag acceleration
D_i	Initial value of drag acceleration
D1, D2, D3	Drag segments
E_f	Final energy at TAEM interface
E_i	Initial energy at re-entry
E_1, E_2	Energies of the boundary values of the constant drag
g_0	Gravitational acceleration at the Earth's surface
h	Height above earth's surface
L	Aerodynamic lift acceleration
m	Mass of the vehicle
n_{max}	Maximum g-load acceleration
q_{max}	Maximum dynamic pressure
$\dot{Q}_{max}$	Maximum heat flux
r	Radial distance from the centre of the Earth to the URSV
R	Earth's radius
R_n	Vehicle nose radius
S_{ref}	Reference surface of the URSV
$\mathbf{u}$	Control vector
V	Velocity of the URSV
V_c	Circular velocity
V_i	Inertial velocity
$\mathbf{x}$	State vector
α	Angle of attack
α_{max}	Maximum value of angle of attack
$\alpha_{(L/D)_{max}}$	Angle of attack for maximum lift to drag ratio
ρ_0	Atmospheric density at sea level
γ	Flight path angle
θ	Geodetic longitude

ρ	Atmospheric density
σ	Bank angle
φ	Geodetic latitude
ψ	Azimuth angle
ΔV	Difference in velocity